Supplementary materials

Intermetallic $MnNi_3$ phase separated from nanoporous nickel as hydrogen evolution electrocatalyst in basic media

Fengping Ning,[a,#] Mei Wang,[a,#,*] Huifang Zhao,[a] Guanshui Ma,[b] Jianfang Meng,[a,c] Ruifeng Dong,[a] Hua Hou,[d,*] Xiaoguang Wang[e,*]

[a] School of Mechanical Engineering & School of Materials Science and Engineering & School of Semiconductor and Physics, North University of China, Taiyuan 030051, China

[b] Key Laboratory of Advanced Marine Materials, Ningbo Institute of Materials Technology and Engineering, Chinese Academy of Sciences, Ningbo 315201, China

[c] Zhejiang Easyclean Environmental Technology Co.,Ltd., Pinghu 314200, China

[d] School of Materials Science and Engineering, Taiyuan University of Science and Technology, Taiyuan 030024, China

[e] Laboratory of Advanced Materials and Energy Electrochemistry, School of Materials Science and Engineering, Taiyuan University of Technology, Taiyuan 030024, China

[#] These authors contributed equally to this work.

* Corresponding author: wangmei@nuc.edu.cn, houhua@nuc.edu.cn, wangxiaog1982@163.com

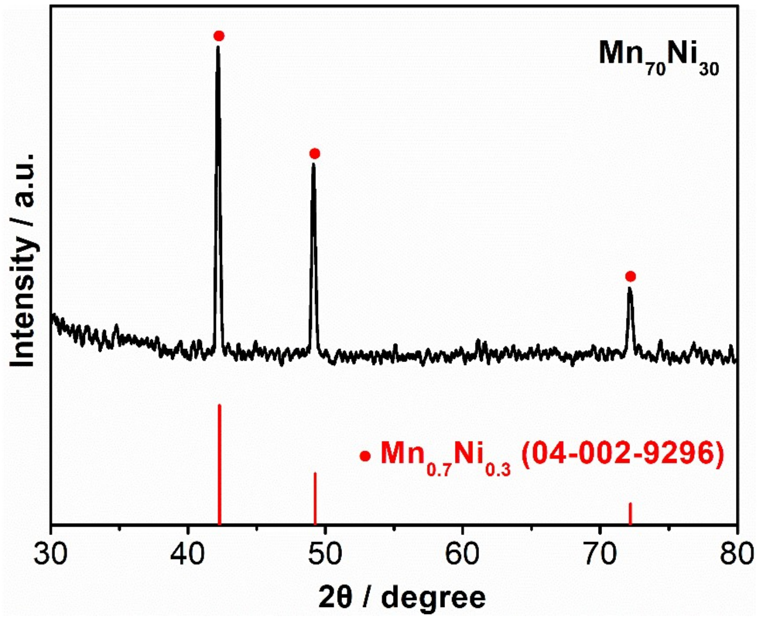

Fig. S1 XRD pattern of $Mn_{70}Ni_{30}$ initial alloy.

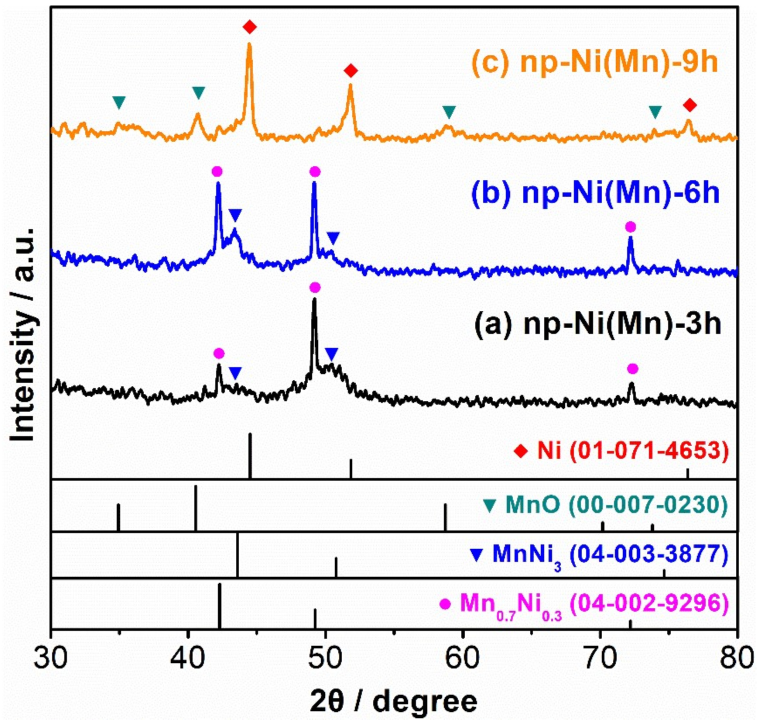

Fig. S2 XRD patterns of dealloyed catalysts: (a) np-Ni(Mn)-3h, (b) np-Ni(Mn)-6h and (c) np-Ni(Mn)-9h.

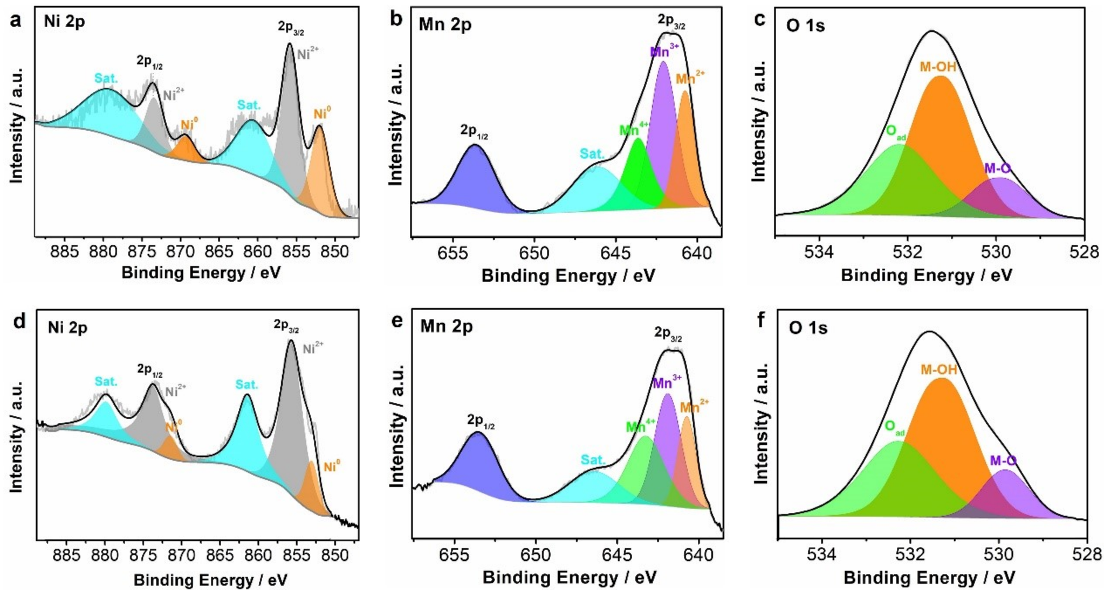

Fig. S3 XPS spectra of $MnNi_3$/np-Ni-3h electrode: (a) Ni 2p, (b) Mn 2p, (c) O 1s. XPS spectra of $MnNi_3$/np-Ni-6h electrode: (d) Ni 2p, (e) Mn 2p, (f) O 1s.

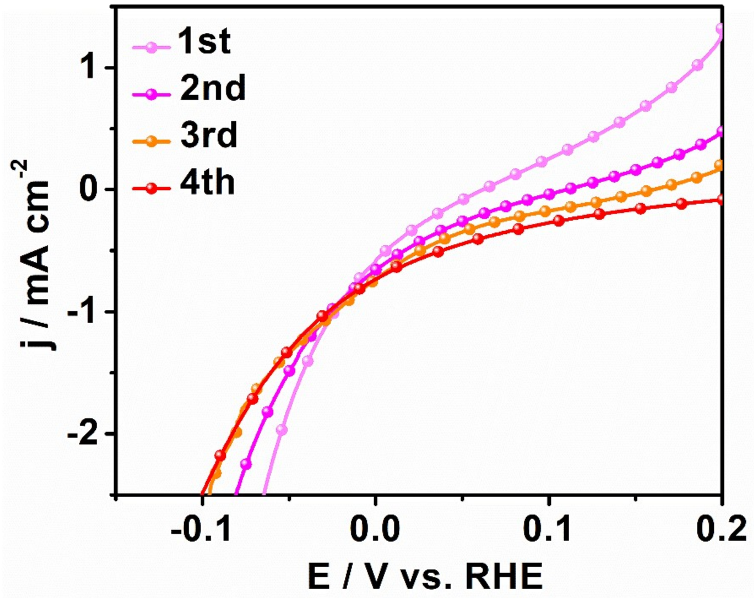

Fig. S4 Initial four LSV curves of $MnNi_3$/np-Ni-9h electrode.

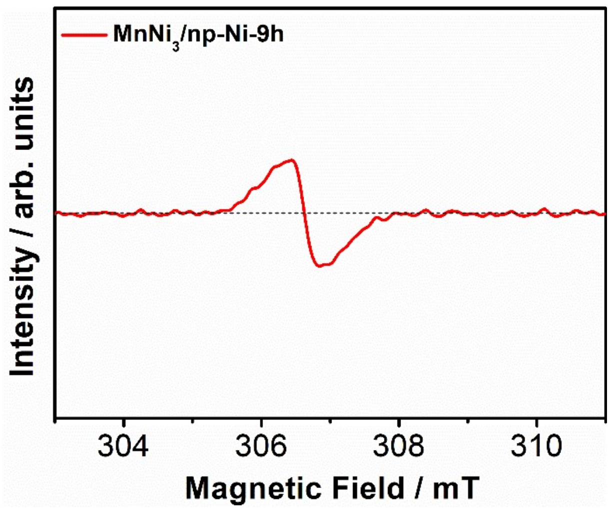

Fig. S5 EPR spectra of $MnNi_3$/np-Ni-9h electrode.

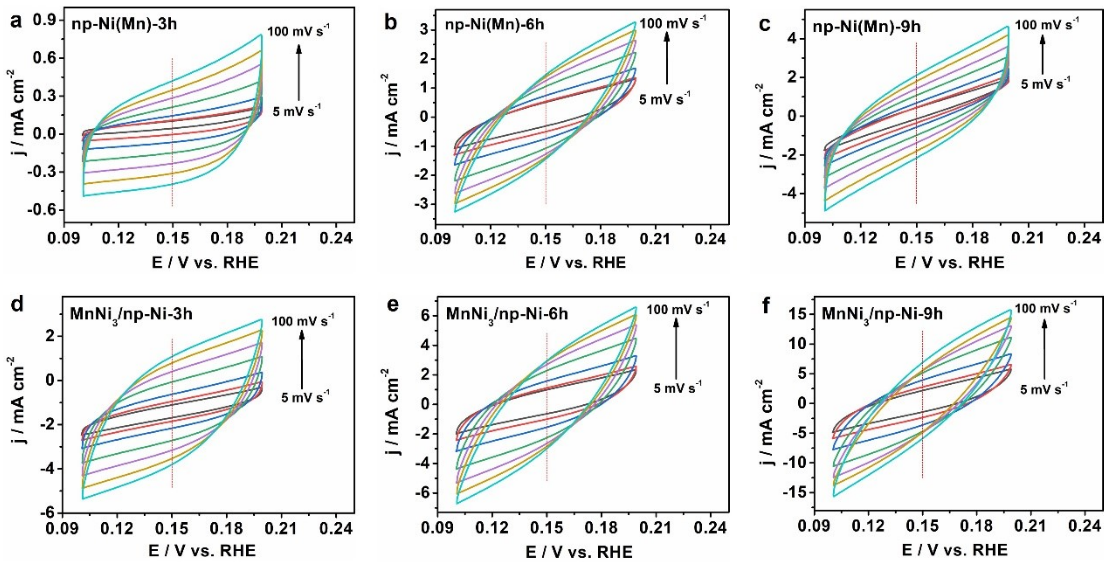

Fig. S6 CV curves (0.1～0.2 V vs. RHE) of (a) np-Ni(Mn)-3h, (b) np-Ni(Mn)-6h, (c) np-Ni(Mn)-9h, (d) $MnNi_3$/np-Ni-3h, (e) $MnNi_3$/np-Ni-6h and (f) $MnNi_3$/np-Ni-9h electrodes under different scan rates (5～100 mV s^{-1}).

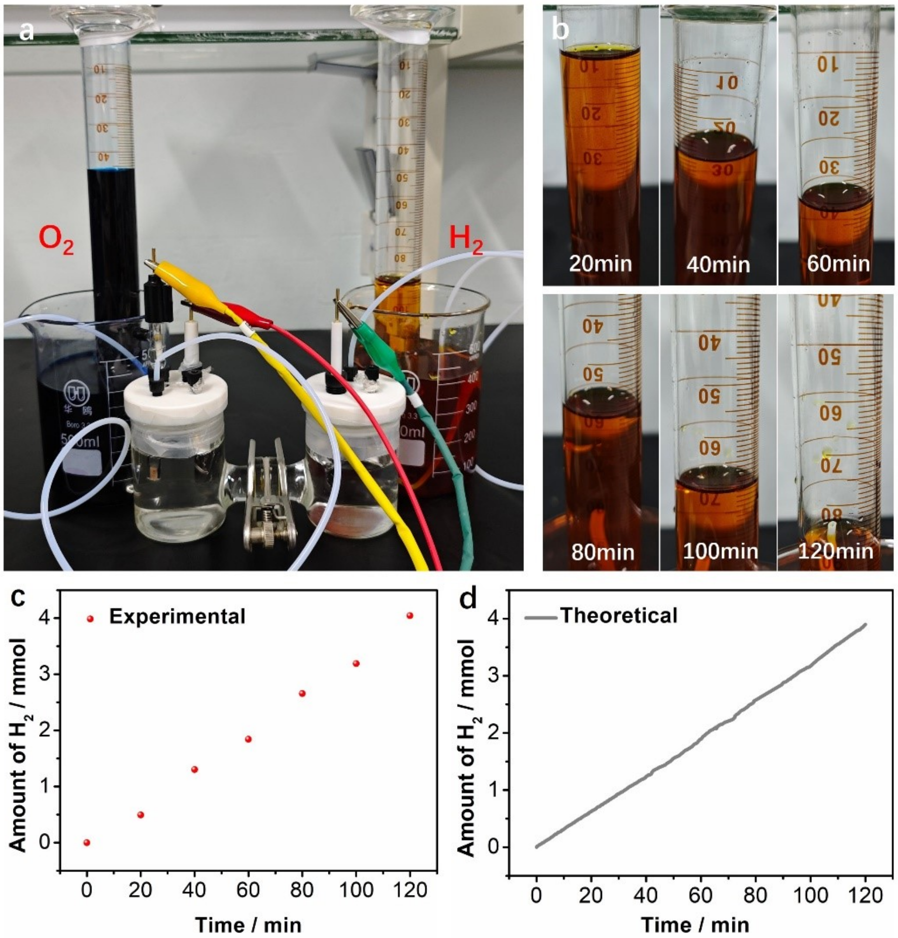

Fig. S7 (a) Photograph of hydrogen production/collection device. (b) Photographs of H_2 yield at constant potential of 300 mV within 120 min. (c) Actual H_2 yield calculated by formula S1. (d) Theoretical H_2 yield calculated by formula S2.

$$n(mol) = \frac{\rho \cdot V}{M} = \frac{0.0899(g/L) \cdot V(L)}{2(g/mol)} \tag{S1}$$

$$n(mol) = \frac{I \cdot t}{2 \cdot F} = \frac{I(A) \cdot t(s)}{2 \cdot 96485} \tag{S2}$$

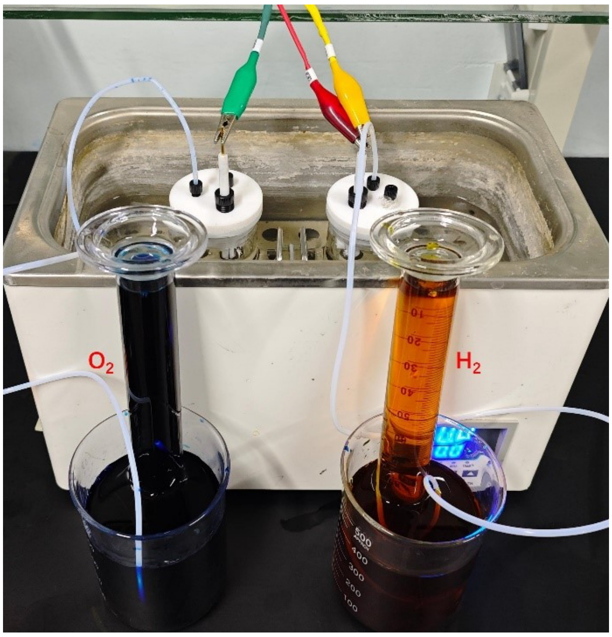

Fig. S8 Photograph of hydrogen production/collection device under industrial conditions (6M KOH, 60 ℃).

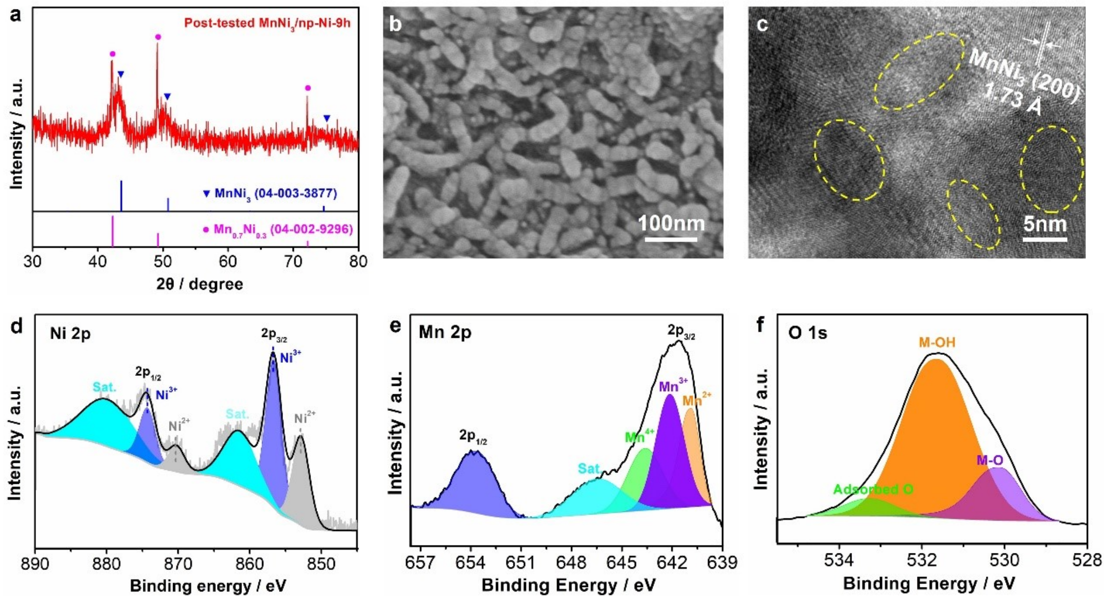

Fig. S9 (a) XRD pattern, (b) SEM image, (c) HRTEM image of post-tested $MnNi_3$/np-Ni-9h. XPS spectra of post-tested $MnNi_3$/np-Ni-9h: (D) Ni 2p, (E) Mn 2p, (F) O 1s.

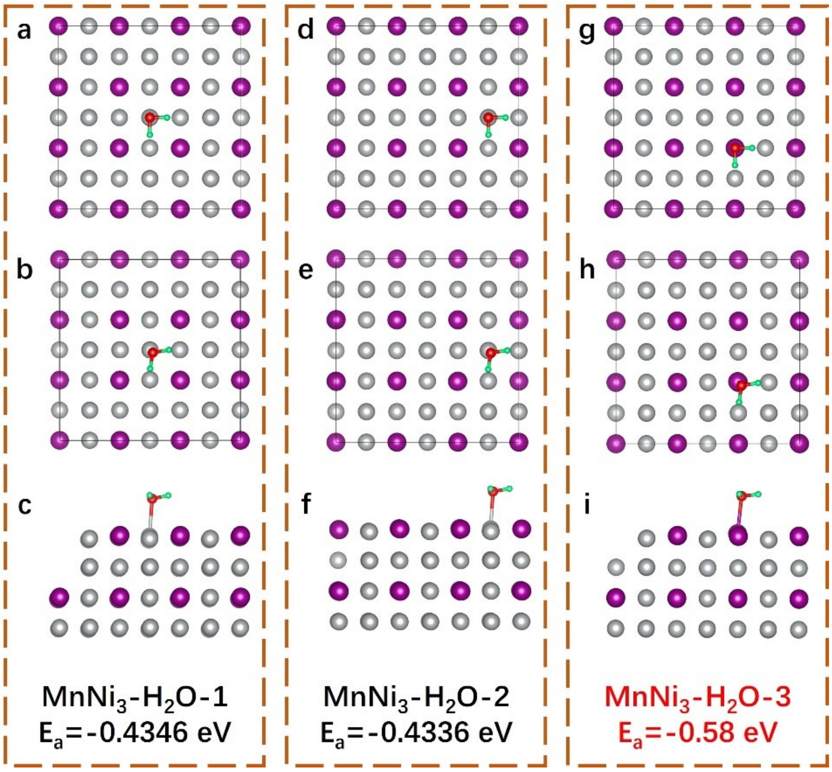

Fig. S10 (a, d, g) *H_2O adsorption models of $MnNi_3$ on different metal sites. (b, e, h) Top view of optimized *H_2O adsorption models. (c, f, i) Side view and corresponding adsorption energies of optimized *H_2O adsorption models.

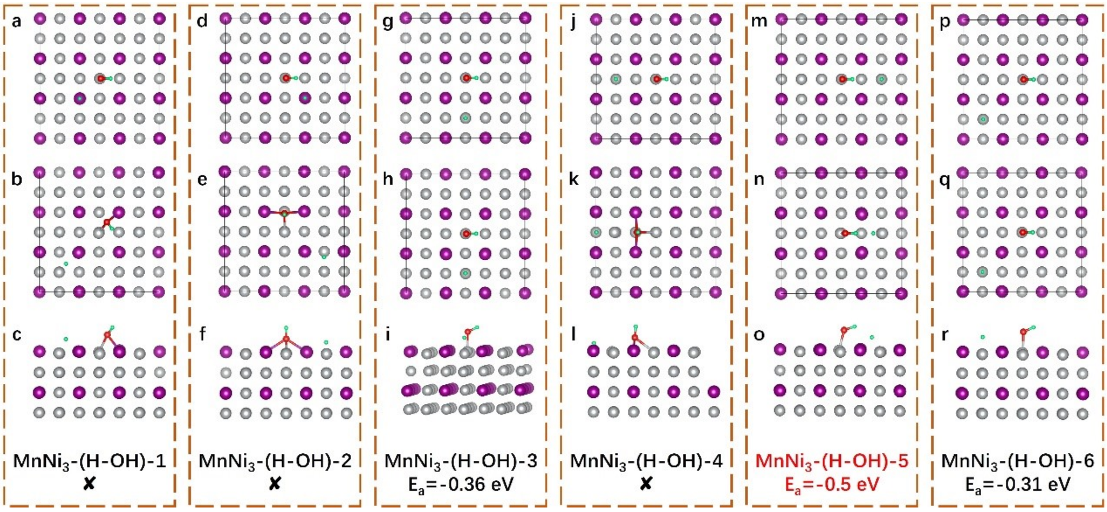

Fig. S11 (a, d, g, j, m, p) *(OH-H) adsorption models of $MnNi_3$ on different metal sites. (b, e, h, k, n, q) Top view of optimized *(OH-H) adsorption models. (c, f, i, l, o, r) Side view and corresponding adsorption energies of optimized *(OH-H) adsorption models.

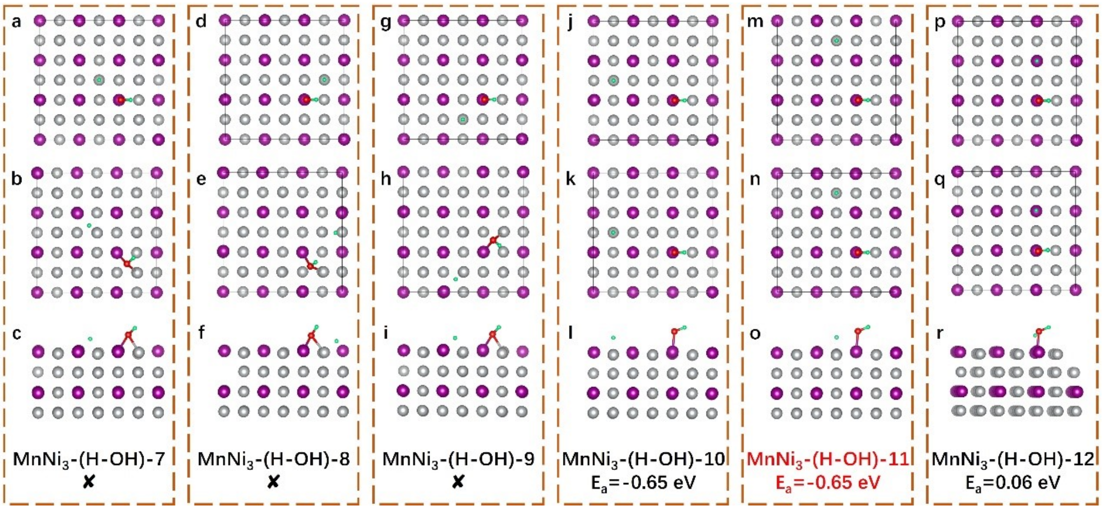

Fig. S12 (a, d, g, j, m, p) *(OH-H) adsorption models of $MnNi_3$ on different metal sites. (b, e, h, k, n, q) Top view of optimized *(OH-H) adsorption models. (c, f, i, l, o, r) Side view and corresponding adsorption energies of optimized *(OH-H) adsorption models.

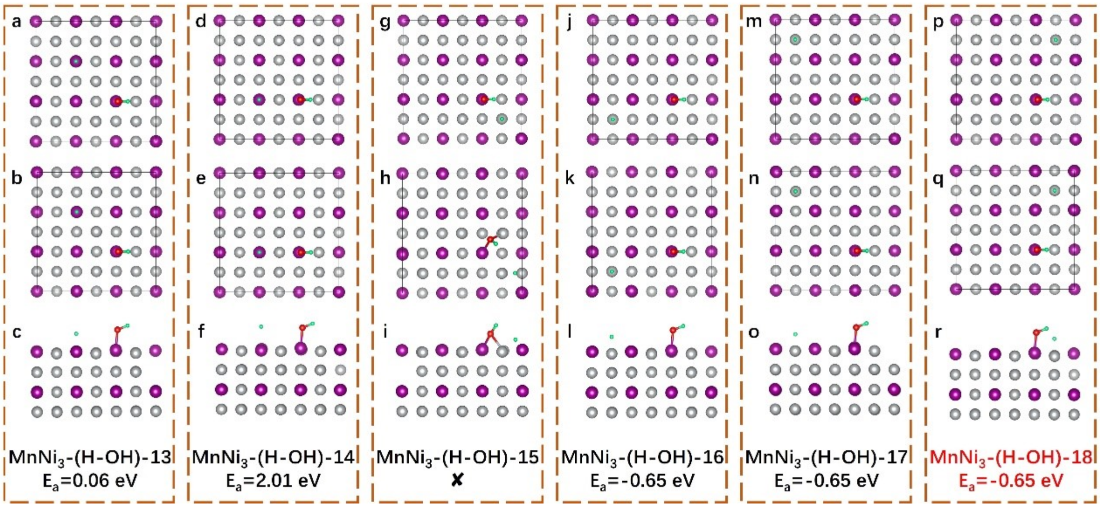

Fig. S13 (a, d, g, j, m, p) *(OH-H) adsorption models of $MnNi_3$ on different metal sites. (b, e, h, k, n, q) Top view of optimized *(OH-H) adsorption models. (c, f, i, l, o, r) Side view and corresponding adsorption energies of optimized *(OH-H) adsorption models.

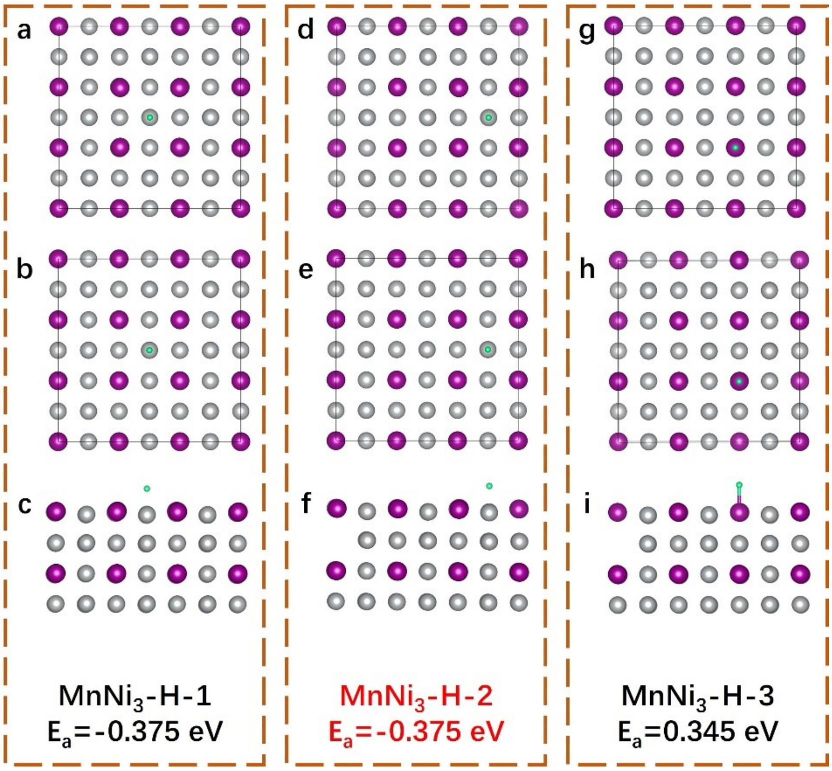

Fig. S14 (a, d, g) *H adsorption models of $MnNi_3$ on different metal sites. (b, e, h) Top view of optimized *H adsorption models. (c, f, i) Side view and corresponding adsorption energies of optimized *H adsorption models.

Table S1 Comparison of HER performance in 1 M KOH for the as-prepared catalysts in this study with the other reported catalysts in literatures.

Catalysts	η_{10} (mV)	Tafel slope (mV dec^{-1})	Reference
np-Ni(Mn)-3h	305	192	This work
np-Ni(Mn)-6h	291	145	
np-Ni(Mn)-9h	228	133	
$MnNi_3$/np-Ni-3h	249	161	
$MnNi_3$/np-Ni-6h	195	119	
$MnNi_3$/np-Ni-9h	**107**	**85**	
Pt/C (m=0.32 mg cm^{-2})	90	93	
Pt/C (m=0.34 mg cm^{-2})	62	68	[1]
Pt/C (m=1 mg cm^{-2})	39	58	[2]
Mo_2C-$Ni(OH)_2$	119	81.4	[3]
Co-1T-MoS_2-bpe	118	83	[4]
NiS@$CoNi_2S_4$/NC	126	47.2	[5]
CoP/MoP@NPC	211	64.6	[6]
Mo_6Co_7-20h	165	--	[7]
N, S-doped Mo_2C-Mo/C	118	74	[8]
$CoSe_2$/Co_3S_4@Co_3O_4	165	117.7	[9]
α-MoB_2	124	61	[10]
MoNiS/$Mo_2TiC_2T_x$	153	92	[11]

Table S2 EIS parameters obtained by fitting the Nyquist plots to the equivalent circuit model in 1 M KOH at -0.1 V vs. RHE.

Catalysts	R_s / Ω	R_0 / Ω	R_{ct} / Ω
np-Ni(Mn)-3h	0.756	—	150.86
np-Ni(Mn)-6h	0.685	—	123.29
np-Ni(Mn)-9h	1.434	—	59.67
$MnNi_3$/np-Ni-3h	1.574	0.417	8.008
$MnNi_3$/np-Ni-6h	0.418	0.346	3.885
$MnNi_3$/np-Ni-9h	0.982	0.308	3.220

Table S3 AWE activities of $MnNi_3$/np-Ni-9h ‖ RuO_2 electrolyzer along with other reported catalysts.

Couple	Cell voltage (V)	Condition	Reference
$MnNi_3$/np-Ni-9h ‖ RuO_2	1.54 V@100 mA cm^{-2} 1.73 V@500 mA cm^{-2} 1.90 V@1000 mA cm^{-2}	60℃, 6M KOH	This work
Ni_2P-$NiMoO_x$/NF ‖ Ni_2P-$NiMoO_x$/NF	1.66 V@100 mA cm^{-2} 2.08 V@400 mA cm^{-2}	65℃, 30% KOH	[12]
$Mo_{0.25}$NiFe ‖ $Mo_{0.25}$NiFe	1.85V@100 mA cm^{-2}	30% KOH	[13]
Fe-Ni_3S_2/PNF-5 ‖ Fe-Ni_3S_2/PNF-5	1.75 V@400 mA cm^{-2}	85℃, 30% KOH	[14]
NiMoB ‖ NiMoB	2.1 V@500 mA cm^{-2}	60℃, 6M KOH	[15]
Ni/MoO_2@CN ‖ Ni/MoO_2@CN	1.73 V@200 mA cm^{-2}	60℃, 6M KOH	[16]
NiCo@C-NiCoMoO/NF ‖ NiCo@C-NiCoMoO/NF	1.8 V@500 mA cm^{-2}	60℃, 6M KOH	[17]
$Fe_{0.14}Co_{0.86}$-P/CC ‖ $Fe_{0.14}Co_{0.86}$-P/CC	1.95 V@500 mA cm^{-2} 2.14 V@1000 mA cm^{-2}	30% KOH	[18]
FeIr/NF ‖ FeIr/NF	1.75 V@500 mA cm^{-2}	60℃, 30% KOH	[19]

References

1 H. Tan, B. Tang, Y. Lu, Q. Ji, L. Lv, H. Duan, N. Li, Y. Wang, S. Feng, Z. Li, C. Wang, F. Hu, Z. Sun and W. Yan, *Nat. Commun.*, 2022, **13**, 2024.

2 H. J. Liu, S. Zhang, Y. M. Chai and B. Dong, *Angew. Chem.,* 2023, **235**, e202313845.

3 H. C. Fu, X. H. Chen, B. Yang, Y. H. Luo, T. Li, X. H. Wang, Q. Zhang, X. L. Li, N. B. Li and H. Q. Luo, *Appl. Catal. B Environ. Energy*, 2023, **332**, 122739.

4 H. J. Liu, S. Zhang, Y. M. Chai and B. Dong, *Angew. Chem. Int. Ed. Engl.*, 2023, **62**, e202313845.

5 J. Dang, S. Yun, Y. Zhang, G. Yang, J. Yang, D. Qiao and T. Yang, *J. Colloid Interface Sci.*, 2023, **630**, 91-105.

6 S. S. Liu, L. J. Ma and J. S. Li, *J. Colloid Interface Sci.*, 2023, **631**, 147-153.

7 Y. Yang, R. Deng, C. Wang, J. Sun, A. K. Iyer, C. C. Laing, H. Yao, S. Ma and M. G. Kanatzidis, *Chem. Mater.*, 2024, **36**, 2566-2576.

8 X. Wang, L. Xia, C. Guo, L. Luo, J. Dai, X. Liu, L. He, C. Yang, Y. Xu, B. Zeng and L. Dai, *Appl. Surface Sci.*, 2023, **614**, 156276.

9 C. Sun, C. Wang, H. Xie, G. Han, Y. Zhang and H. Zhao, *Small*, 2023, **19**, e2302056.

10 X. Liu, Y. Gong, *ACS Appl. Nano Mater.*, 2022, **5**, 10183-10191.

11 J. Zhang, W. Zhang, J. Zhang, Y. Li, Y. Wang, L. Yang and S. Yin, *J. Alloys Compd.*, 2023, **935**, 167974.

12 J.-T. Ren, L. Chen, H.-Y. Wang, W.-W. Tian, X.-L. Song, Q.-H. Kong and Z.-Y. Yuan, *ACS Catal.*, 2023, **13**, 9792-9805.

13 N. S. Gultom, T.-S. Chen, M. Z. Silitonga and D.-H. Kuo, *Appl. Catal. B Environ. Energy*, 2023, **322**, 122103.

14 B. Zhong, B. Cheng, Y. Zhu, R. Ding, P. Kuang and J. Yu, *J. Colloid Interface Sci.*, 2023, **629**, 846-853.

15 R. Mandavkar, M. A. Habib, S. Lin, R. Kulkarni, S. Burse, J.-H. Jeong and J. Lee, *Appl. Mater. Today*, 2022, **29**, 101579.

16 G. Qian, J. Chen, T. Yu, J. Liu, L. Luo and S. Yin, *Nanomicro Lett.*, 2021, **14**, 20.

17 G. Qian, J. Chen, T. Yu, L. Luo and S. Yin, *Nanomicro Lett,*, 2021, **13**, 77.

18 H. Yu, L. Qi, Y. Hu, Y. Qu, P. Yan, T. T. Isimjan and X. Yang, *J. Colloid Interface Sci.*, 2021, **600**, 811-819.

19 J. Chen, Y. Wang, G. Qian, T. Yu, Z. Wang, L. Luo, F. Shen and S. Yin, *Chem. Eng. J.*, 2021, **421**, 129892.